Oblique Propagation of Monsoon Gravity Waves During the Northern Hemisphere 2007 Summer

Brentha Thurairajah[1], David E Siskind[2], Scott M Bailey[1], Justin N Carstens[1], James M Russell III[3], Martin G. Mlynczak[4]

[1]Center for Space Science and Engineering Research, Bradley Department of Electrical and Computer Engineering, Virginia Tech, Blacksburg, Virginia, USA

[2]Space Science Division, Naval Research Laboratory, Washington DC, USA

[3]Center for Atmospheric Sciences, Hampton University, Hampton, Virginia, USA

[4]NASA Langley Research Center, Hampton, Virginia, USA

Corresponding Author: Brentha Thurairajah (brenthat@vt.edu)

Key Points:

- Gravity wave momentum flux from satellite and model data exhibit a poleward tilt from the tropics to the poles in the NH summer
- Slanted structure of the correlation coefficient between the 50 km tropical monsoon GWs and the easterly winds indicate oblique propagation
- During the NH 2007 PMC season the tropical monsoon GW activity is positively correlated to the PMC occurrence frequency

Abstract

We present a combination of satellite observation and high-resolution model output to understand monsoon convection as a source of high-latitude mesospheric gravity waves (GWs). The GWs generated over the Northern Hemisphere (NH) monsoon region during the 2007 summer and the role of the winds in focusing these GWs toward the high-latitude middle atmosphere are analyzed using the SABER/TIMED satellite temperature data and the high-resolution NOGAPS-ALPHA model results. In the NH, above the stratosphere, the monsoon GW momentum flux (GWMF) exhibits a poleward tilt that follows the slanted structure of the easterly jet. The correlation coefficients (> 0.5) between the time series of NH tropical stratospheric GWMF and the global winds also have a slanted structure that tracks the easterly jet, confirming the modeling theory that stratospheric monsoon GWs are refracted into the summer easterly jet and can reach the high-latitude mesosphere. Since Polar Mesospheric Clouds (PMCs) are sensitive indicators of changes in the polar summer mesosphere, we compared the time series of tropical stratospheric GWMF to the PMC occurrence frequency (OF) obtained from the CIPS/AIM satellite data, to assess the influence of this wave focusing in the mesosphere. There is a significant positive correlation between the high latitude PMC OF and the tropical stratospheric GWMF indicating a definite influence of monsoon GWs on the high-latitude mesosphere. The disagreement in correlation at the end of the PMC season is attributed to the enhancement of the quasi 5-day planetary wave dominating over the influence of monsoon GWs on PMCs.

Keywords: Gravity Waves, Oblique Propagation, Polar Mesospheric Clouds, Monsoon Gravity Waves

1. Introduction

Atmospheric Gravity Waves (GWs) play an important role in the general circulation of the atmosphere. Vertically propagating GWs carry momentum from their source and can exert a zonal force on the background flow by transferring their momentum through wave breaking and dissipation. The zonal force exerted by GWs on the mesosphere induces a pole-to-pole residual circulation that is responsible for the cold summer mesosphere and warm winter mesosphere [e.g. *Lindzen*, 1981; *Holton and Alexander*, 2000]. Polar Mesospheric Clouds (PMCs), the highest clouds on Earth (~84 km) form in this cold summer mesosphere and are of interest owing to their sensitivity to changes in the mesospheric environment. The PMC variability in response to changes in its environment can be used to understand long-term changes in the mesosphere [e.g. *Hervig* et al., 2016] and clarify their response, if any, to global climate change [*Thomas* et al., 1989; *von Zahn*, 2003; *Thomas* et al., 2003].

One of the classic problems in middle atmospheric science is how to properly represent GWs in global models. GWs are parametrized in most models, since the spatial scales of GWs are typically smaller than the grid spacing of the model [*Garcia and Solomon*, 1985; *Alexander and Dunkerton*, 1999; *Kim* et al., 2003; *Siskind* et al., 2003; *Garcia* et al., 2007; *Richter* et al., 2010]. A key assumption of the various GW parameterization schemes is that only vertical wave propagation is considered. However, this assumption of vertical propagation in GW parametrization schemes has recently been called into question [*Buhler and McIntyre*, 2003; *Hasha* et al., 2008; *Preusse* et al., 2009]. *Sato* et al. [2009] used a gravity wave resolving model and showed that in summer, convection from monsoon regions was the largest source of GWs and that due to the latitudinal shear in the prevailing easterly wind, these waves would be refracted poleward. *Sato* et al. [2009] suggested that these monsoon GWs tend to focus into the mesospheric jet, and as the waves propagate vertically they decelerate the jet and contribute to the slanted structure of the easterlies. This easterly jet associated with the monsoon circulation is slanted toward the high-latitudes and could allow the oblique propagation of monsoon GWs from the low-latitude monsoon region to the high-latitude mesosphere.

Observational studies by *Sato* et al. [2003] using radiosonde data, and by *Jiang* et al. [2004] and *Ern* et al. [2011] using satellite data have also suggested the possibility of lateral propagation of GWs from their source of tropical convection to the high-latitude upper stratosphere and lower mesosphere, in the summer hemisphere. The consequence of latitudinal (also referred as lateral, oblique, non-vertical) propagation of GWs on calculated gravity wave drag was explored by *Kalisch* et al. [2014] using the Gravity wave Regional Or Global RAy Tracer (GROGRAT) ray-tracing model. Most recently, *Yasui* et al. [2016] reported a positive correlation between GWs derived from mesospheric (72-76 km) wind data from Syowa Station (69°S) in Antarctica and precipitation data in December and January from the tropics (10-20°S, 0-80°E) and suggest that "a significant component of the mesospheric GWs in the SH polar region originated and propagated poleward from the tropical convection".

Since PMCs are known to be sensitive to the temperature of the cold summer mesopause, which in turn can be influenced by the obliquely propagating gravity waves originating at low latitudes, it is reasonable to investigate whether this linkage between PMCs and low latitude gravity waves can be documented more directly. However, it is important to recognize, as discussed by for e.g. *Gerrard* et al. [2004], that GWs can have two opposing effects on PMCs. Globally, GWs act to cool the summer mesosphere by driving the winter to summer mean meridional circulation. In this case, increased gravity waves would correlate with an increase in occurrence of PMCs. Locally, GW induced temperature fluctuations can either cause PMCs to sublimate and thus reduce cloud occurrence in the warm phase of the wave or temporarily increase PMC occurrence in the cold phase [e.g. *Jensen and Thomas*, 1994; *Rapp* et al., 2002; *Gerrard* et al., 2004; *Chandran* et al., 2010]. *Jensen and Thomas* [1994] used the Community Aerosol and Radiation Model for Atmospheres (CARMA) model to show that the net effect of GW induced temperature is a decrease in PMC albedo. *Rapp* et al. [2002] used an updated version of CARMA to show that GWs with wave periods longer than 6.5 hours amplified PMCs while shorter period waves destroyed PMCs. In agreement with these modelling studies, *Chandran* et al. [2010] used satellite observations to show that short period GWs tend to destroy PMCs, as dissipating GWs increased the temperature at PMC altitudes. In addition, various lidar studies have shown either a decrease in cloud occurrence with increasing stratospheric GWs or no relationship between GW activity and mesospheric clouds [*Gerrard* et al., 2004; *Innis* et al., 2008; *Chu* et al., 2009].

In this paper, we present a combination of observation and modeling study to understand the propagation of monsoon generated GWs, the contribution of the summer easterly winds to the propagation direction, and the influence of these GWs on the summer polar mesosphere during the NH 2007 summer. We derive GW parameters (momentum flux and amplitude) from temperature observations from the Sounding of the Atmosphere using Broadband Emission Radiometry (SABER) instrument onboard the Thermosphere Ionosphere Mesosphere Energetics and Dynamics (TIMED) satellite. The Navy Operational Global Atmospheric Prediction System - Advanced Level Physics High Altitude (NOGAPS-ALPHA) model results are used to calculate the GW momentum flux, analyze the direction of wave propagation, and to study of the role of winds in the filtering and propagation of GWs. Since PMCs are sensitive to changes in their environment, and their structures and annual variation have been used to understand the dynamics of the polar summer mesosphere [e.g. *Dalin* et al., 2004; *Karlsson* et al., 2009; *Nielsen* et al., 2010; *Chandran* et al., 2010; *Thurairajah* et al., 2013], we use PMC observations from the Cloud Imaging and particle Size (CIPS) experiment onboard the Aeronomy of Ice in the Mesosphere (AIM) satellite, as an indicator of the changes in the summer mesospheric environment.

This paper is organized as follows. Section 2 contains a description of the data and method used to derive GW momentum flux from satellite data. The global GW characteristics from SABER and NOGAPS-ALPHA are presented in Section 3. The role of winds in the oblique propagation of monsoon GWs is presented in Section 4. The influence of these GWs on PMCs is presented in Section 5. Section 6 contains a discussion, and Section 7 describes a summary and conclusions.

2. Data and Method

2.1 SABER

SABER is a limb-scanning infrared radiometer that measures global temperature, pressure, geopotential height, and trace species from ~10-110 km [*Russell* et al., 1999]. SABER temperature data are available since 2002, with continuous measurements over the latitude range 50°N-50°S (this includes the monsoon region). In the Northern hemisphere (NH) summer, high-latitude measurements are limited to the first half of summer (i.e. 15 May to 15 July) owing to the periodic yaw maneuvers in the TIMED satellite. This does not pose a problem to our study as this time period includes half the PMC season and is sufficient to confirm the poleward tilt of the monsoon GWMF. In this study we use the version 2.0 level 2 data product.

Satellite temperature observations have been proven to be a valuable resource of global GW parameters [*Wu* et al., 2006 and references therein], albeit being limited to observing only a part of the GW spectrum owing to the observational filter of that particular instrument [e.g. *Alexander* et al., 2010]. GW parameters (e.g. momentum flux, amplitude) derived from SABER temperature data have been validated and demonstrated to be reliable for GW related studies [e.g. *Preusse* et al., 2009; *Ern* et al., 2011; *Yamashita* et al., 2013 and references therein]. *Ern* et al. [2004] first demonstrated the feasibility of using temperature data from the CRyogenic Infrared Spectrometers and Telescopes for the Atmosphere (CRISTA), a limb-viewing instrument, to calculate the total vertical flux of horizontal momentum due to GWs. The authors started from the *x* (zonal) and *y* (meridional) components (*Fpx*, *Fpy*) of the GW Momentum Flux (GWMF) vector (from equation 41 in *Fritts and Alexander* [2003]) given by,

$$Fpx, Fpy = \rho\left(1 - \frac{f^2}{\widehat{\omega}^2}\right)\left(\overline{u'w'}, \overline{v'w'}\right) \qquad (1)$$

where, ρ is the density of the background atmosphere, *f* is the coriolis parameter, $\widehat{\omega}$ is the intrinsic frequency, and u', v', and w' are the perturbation zonal, meridional, and vertical winds, respectively. The total vertical flux of horizontal momentum is,

$$Fph = \sqrt{Fpx^2 + Fpy^2} \qquad (2)$$

Ern et al. [2004] then used a mid-frequency approximation ($N \gg \widehat{\omega} \gg f$) to derive the GWMF appropriate for use with satellite temperature data (a complete derivation is given in the Appendix of their paper), given by

$$GWMF = \frac{1}{2}\rho\frac{k}{m}(g/N)^2\left(\frac{\hat{T}}{T_o}\right)^2 \qquad (3)$$

where, *k* is the horizontal wavenumber, *m* is the vertical wavenumber, *g* is the acceleration due to gravity, *N* is the Brünt Vaisala frequency, $\hat{T}$ is the temperature amplitude, and T_o is the background temperature. In the present study, each temperature profile (binned into 2.5° latitude x 24° longitude) is fit with a least squares fit, estimated by first fitting a third-order polynomial to the logarithm of each temperature profile [e.g. *Thurairajah* et al., 2014]. A residual is calculated by subtracting the fitted profile from the logarithmic profile, and filtered with a 4 km boxcar filter to remove noise. The filtered residual is then added back to the polynomial fit, and the antilog of the resulting profile is considered the least squares fit. These fitted profiles are used to calculate the background temperature (T_o) as the sum of the zonal mean temperature (wavenumber, WN 0) and PW components (WN 1-5) [e.g. *Preusse* et al., 2002; *Yamashita* et al., 2013; *Thurairajah* et al., 2014]. T_o is subtracted from each temperature profile to get the perturbation temperature, *T'*. There is only a small difference in *T'* profiles calculated by subtracting the WN 0-5 components and 0-6 components [*Yamashita* et al., 2013]. A wavelet analysis is used on each *T'* profile to calculate up to three dominant vertical wavelengths (λ_z). These wavelengths are then used to fit sine waves (harmonic fit) in 20 km sliding windows to estimate the amplitude ($\hat{T}$) and phase of the GW.

Only those waves with dominant vertical wavelengths between 4 and 30 km are considered. This effectively removes the influence of equatorial Kelvin waves (λ_z ~3-4.5 km) [*Holton* et al., 2001], quasi-stationary planetary waves, and semi-diurnal and ter-diurnal tidal components (λ_z > 30 km) [e.g. *Forbes* et al., 1994; *Andrews* et al., 1987]. The removal of the WN 1-5 components also reduces the influence of some diurnal tidal components [e.g. *Ern* et al., 2011] and the quasi 2-day wave (WNs 2, 3, 4) [*Salby*, 1981; *Wu* et al., 1993]. Most of the quasi two-day waves derived from SABER data have been shown to have vertical wavelengths longer than 30 km [*Huang* et al., 2013]. Thus the resulting amplitudes, after harmonic fitting, are considered to represent the GW amplitude only.

The phase shift between two adjacent profiles is used to calculate the horizontal wavelength [*Ern* et al., 2011]. Analytical calculations suggest that SABER is sensitive to GWs with horizontal wavelengths greater than 100-200 km [e.g. *Preusse* et al., 2002; *Preusse* et al. 2009]. However, since the horizontal wavelength is calculated from two successive profiles under the assumption that the satellite measurement track and the wave vector are aligned (this might not always be the case), the calculated values are generally overestimated (see for e.g. *Alexander* et al., 2010; *Alexander*, 2015 and references therein). Thus, the longer horizontal distances between profile pairs will lead to an overestimation of horizontal wavelengths (due to under sampling of waves with very short wavelengths) and an underestimation of the gravity wave momentum fluxes. However, equation (1) captures the overall global characteristics of GWs and is dependable for GW studies.

2.2 CIPS

CIPS is an ultraviolet imager that images the atmospheric and PMC radiance from ~40-85° latitude in the summer hemisphere [*McClintock* et al., 2009; *Rusch* et al., 2009; *Bailey* et al., 2009]. PMC data, available in the NH since the summer of 2007, is reported in terms of particle radius, cloud albedo, ice water content, and total number of cloud observations. For our analysis we use the v04.20 level 3c summary files, averaged over the 65-85° latitude band, to calculate the cloud occurrence frequency (OF) as,

$$OF = 100 \times \left(\frac{\sum cloud\ observations}{\sum all\ observations}\right)\% \qquad (4)$$

CIPS PMC retrievals have been validated thorough comparison to SBUV satellite data [*Benze* et al., 2009; 2011]. A detailed description of CIPS data products, including calibration and retrieval algorithms, and a discussion of uncertainties can be found in *Lumpe* et al. [2013] and *Carstens* et al. [2013].

2.3 NOGAPS-ALPHA

The NOGAPS-ALPHA model [*Hoppel* et al., 2008; *Eckermann* et al., 2009] is a high-altitude forecast/analysis model that assimilates observational data from SABER (temperature) and the Microwave Limb Sounder (MLS; temperature, ozone, and H_2O) to provide a synoptic analysis of the atmosphere from 1000 – 0.001 hPa (0 to about 92 km) with a 6 hourly update cycle. NOGAPS-ALPHA is a spectral model and the analysis was produced at a triangular truncation at 79 wavenumbers (T79, about 2.25° x 2.25° in latitude and longitude spatial resolution). We use the zonal wind data from the T79 NOGAPS-ALPHA analysis to understand the role of winds in the oblique propagation of monsoon GWs during the PMC season.

In addition, the NOGAPS-ALPHA analysis was used by *Siskind* [2014] to initialize a series of 10-day forecast runs, without including any parameterized GW drag, at higher spatial resolution (at both T239, about 0.75° resolution and T479, about 0.375° resolution). These resolutions are on the order of other GW resolving models [e.g. *Watanabe* et al., 2008; *Liu* et al., 2014]. *Siskind* [2014] confirmed that increasing the spatial resolution resolved a greater portion of the GW spectrum. Consistent with this, the forecast bias for such GW driven features such as the warm winter stratopause and the cold summer mesopause was progressively reduced for the higher resolution models. Nonetheless, even at T479 a residual bias remained, suggesting the importance of GWs with horizontal spatial scales less than ~120 km on the global circulation. *Liu* et al. [2014] reached a similar conclusion using the high-resolution Whole Atmosphere Community Climate Model (WACCM). Note that the resolving limit of the NOGAPS T479 resolution is similar to the SABER horizontal wavelength sensitivity of values greater than 200 km [*Preusse* et al., 2002].

We use the temperature and wind data from the 10-day high-resolution (T479) NOGAPS-ALPHA forecast initialized on 30 June 2007, to calculate the global vertical GWMF (using equation (3)), and the zonal ($x = \rho u'w'$) and meridional ($y = \rho v'w'$) components. The x and y components provide the direction of propagation of the GWs. Figure 1 shows an example of the zonal component of the GWMF at ~11 hPa (~28 km) for 2 July 2007. High wave activity is seen over the Indian sub-continent, parts of south Asia, South China Sea and West Africa. All these areas have been identified as monsoon regions [*Li and Zeng*, 2002] in the NH and the associated convection is a large source of GWs in the summer.

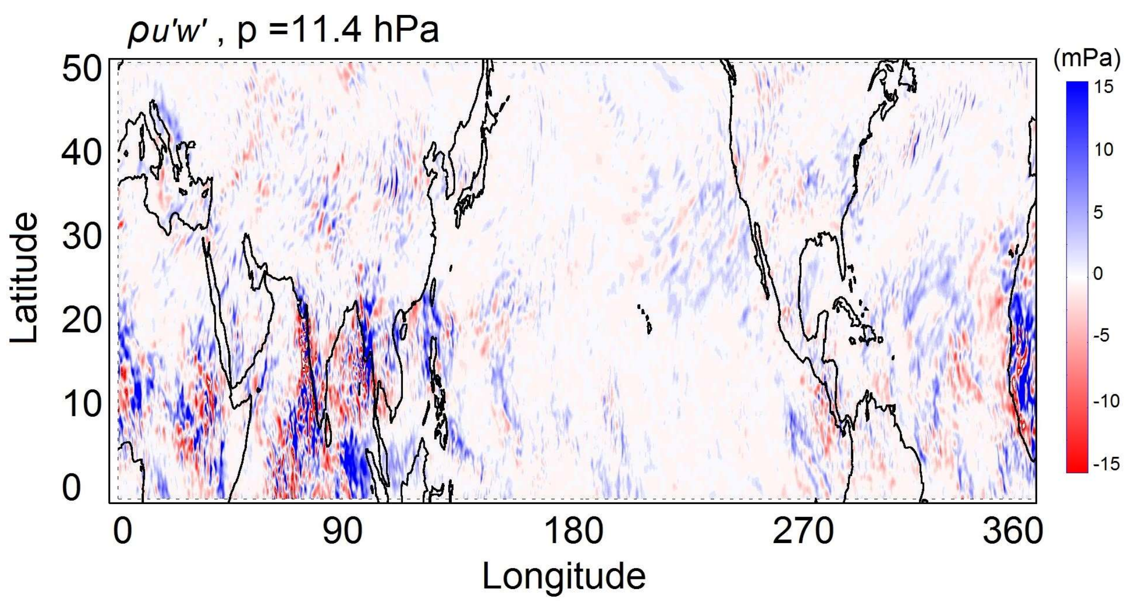

Figure 1. Zonal component of the GWMF in the NH on 2 July 2007 from the high-resolution NOGAPS-ALPHA model.

3. Gravity wave activity during the NH 2007 summer

To understand the middle atmospheric GW activity during the NH summer of 2007, we show in Figure 2 the zonal mean GWMF and squared GW amplitude calculated from SABER temperature, as a function of latitude and altitude for July 2007. The zonal winds from the NOGAPS-ALPHA analysis data are also shown. In general, GWMF decreases with increasing altitude indicating dissipation at all altitudes. The growth in wave amplitude with increasing altitude is due to the decrease in atmospheric density, i.e. effect of energy density conservation. The maximum in GWMF over the NH tropical stratosphere is attributed to the GWs generated from the monsoon region, and over the SH high latitudes (>50°S) to the winter polar vortex [*Ern* et al., 2011]. The zonal winds are easterly (negative) in summer and westerly (positive) in winter. Figure 2 also shows that, in the NH, the GWMF (and amplitude) above ~50 km and the easterly winds have a slanted structure with increasing height. The maximum in momentum flux shifts poleward with increasing altitude and follows the slanted structure of the easterly jet. Note that this tilt was also reported by *Ern* et al. [2011] using SABER data from 2002, and the authors noted the similarity between this poleward shift and the lateral propagation of GWs reported using modelling studies by *Sato* et al. [2009] and *Preusse* et al. [2009]. *Ern* et al. [2011] also stated that this poleward shift in GWMF with height is real and not a manifestation of limb-viewing instruments viewing different portion of the spectrum at different altitudes, as this has been shown to be of little significance in limb-viewing instruments [*Preusse* et al., 2006]. In Figure 2b, the GW amplitudes above 50 km in the tropics and the amplitudes of the slanted structure are at least twice the reported temperature random errors. As an example, a comparison between the precision of SABER version 2.0 temperature data at various altitudes and the corresponding zonal mean amplitudes at 50°N and 80°N, for July 2007, are given in Table 1.

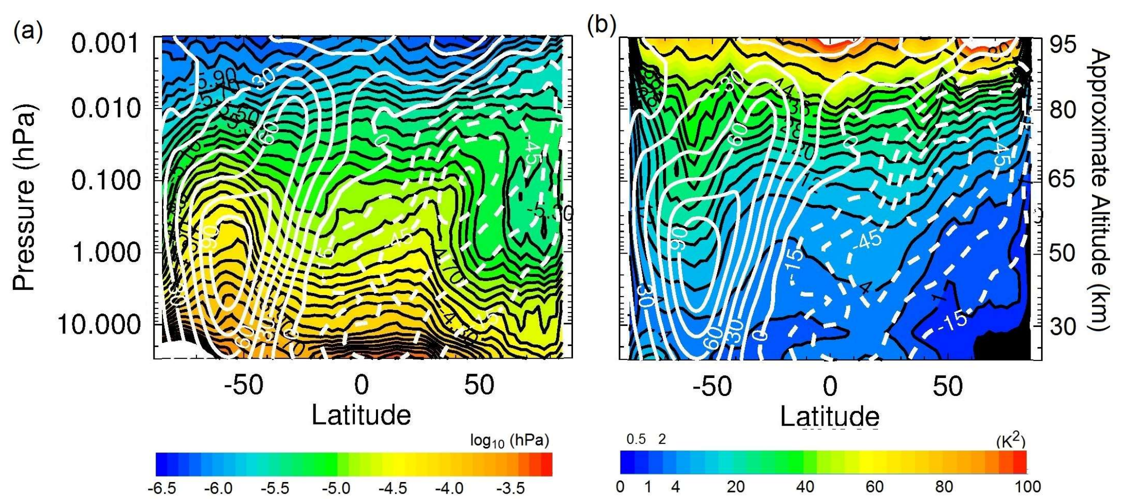

Figure 2. Zonal mean gravity wave (a) momentum flux and (b) squared amplitude for July 2007 from SABER temperature data. The white contours are zonal winds from NOGAPS-ALPHA analysis data. The dashed white contours indicate easterly (negative) winds and the solid white contours indicate westerly (positive) winds.

Above 70 km, at all NH latitudes the amplitude is at least twice the random error or higher. These reasons along with the fact that the amplitude calculations are not susceptible to errors from overestimation of horizontal wavelength (i.e. unlike GWMF calculations), gives us confidence that this slanted structure is real. Note that the SABER operational temperature random errors reported here are errors that have been updated for version 2.0 and are based on studies by *Remsberg* et al. [2008] and *Garcia-Comas* et al. [2008] for the previous released version. These errors are available on the SABER website.

Table 1. SABER temperature precision and GW amplitude

Altitude (km)	Temperature Precision (K)[a]	GW Amplitude at 50°N (K)[b]	GW Amplitude at 80°N (K)[b]
50	0.6	1.1	0.9
60	0.7	1.7	1.3
70	1.0	3.2	2.4
80	1.4	4.7	4.5

[a] SABER version 2 temperature

[b] Zonal mean amplitude for July 2007

To further validate the GWMF calculated from SABER, we show in Figure 3a the mean GWMF calculated from the NOGAPS-ALPHA high-resolution (T479) temperature data available for the first nine days of July 2007 (i.e. data from a 10-day forecast run initialized on June 30). The GWMF has been calculated using equation (3) and the same method described in section 2.1. The momentum flux values from both SABER and NOGAPS-ALPHA are similar in magnitude and show the general characteristics of decrease in GWMF with altitude. The NH GWMF from NOGAPS-ALPHA also exhibits a slanted structure focused into the easterly jet, but this slanted structure is not as well defined as that seen in the SABER GWMF in Figure 2a. To enumerate the differences, in Figure 3b we show the ratio of the GWMF calculated from SABER (Figure 2a) to that from NOGAPS-ALPHA (Figure 3a). In general, the two values are within 5% of each other. Somewhat greater differences are observed in the NH polar mesosphere and SH stratosphere where, as we have noted, the forecast model is known to contain biases. However, given that the GWMF values from SABER and NOGAPS-ALPHA are remarkably similar (i.e. the values of the ratio are generally between 0.78 and 1.02), gives us further confidence that the GWMF features in Figure 2 can be reliably used in this study.

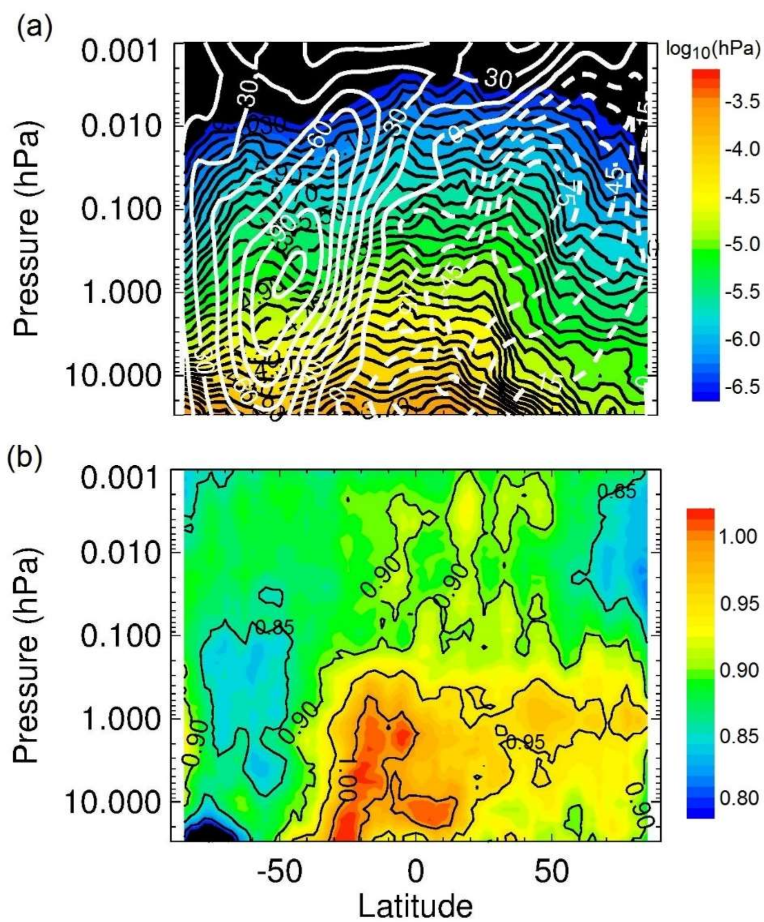

Figure 3. (a) Zonal mean gravity wave momentum flux from NOGAPS-ALPHA averaged over the first 9-days of July 2007 and (b) the ratio of the momentum fluxes from SABER and NOGAPS-ALPHA, for July 2007. The dashed white contours in (a) indicate easterly (negative) winds and the solid white contours indicate westerly (positive) winds.

As noted previously, since the horizontal wavelengths are determined from a pair of adjacent temperature profiles and the satellite measurement track and the gravity wave vector may not necessarily be aligned, the calculation of GWMF from equation (3) gives us an estimate of the absolute value of GWMF and not the direction of wave propagation [*Ern* et al., 2011]. To estimate the wave propagation direction, we use the high-resolution (T479) NOGAPS-ALPHA wind data to calculate the zonal (Figure 4a) and meridional (Figure 4b) components of the GWMF averaged over the first nine days of July 2007. Note that Figure 4a is similar to the 10-day averaged momentum flux shown in *Siskind* [2014], but for a different forecast run (i.e. this run was initialized on June 30). Above ~10 hPa, the SH is characterized by westward and southward propagating GWs and the NH by eastward and northward propagating GWs. At lower altitudes, the GWs are eastward and southward except for a small region in the SH tropics. The eastward and northward propagating waves in the NH stratosphere and mesosphere exhibit the same poleward tilt with increasing altitude seen in the SABER data, confirming the lateral

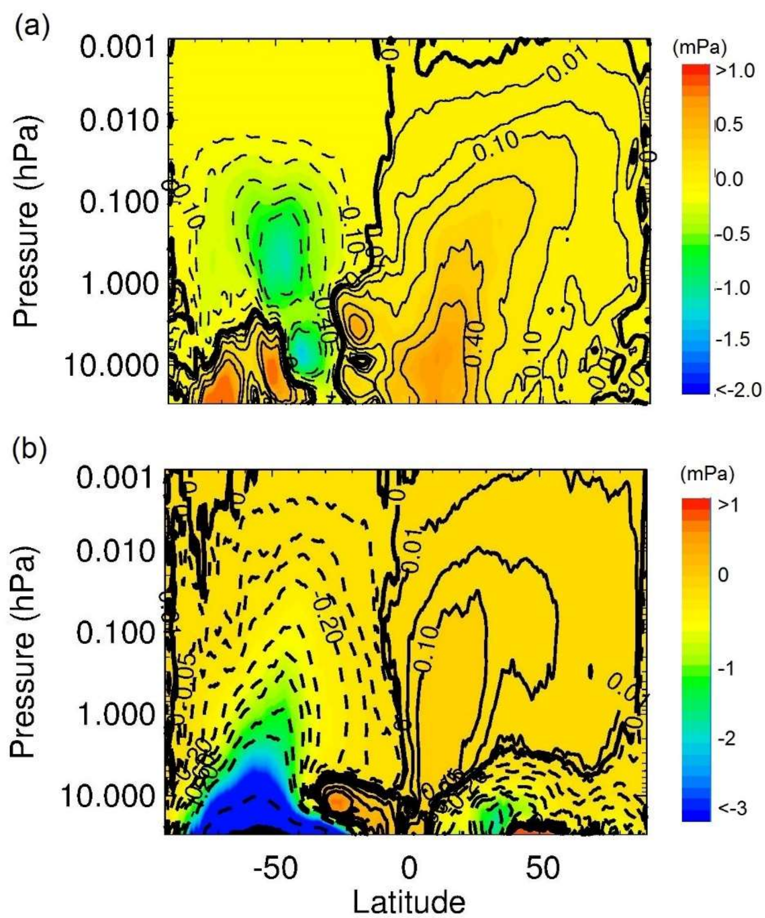

Figure 4. (a) Zonal and (b) meridional components of the zonal mean vertical flux of horizontal momentum of GWs from NOGAPS-ALPHA averaged over the first 9-days of July 2007. The solid contours represent eastward (northward) GWMF, while the dashed contours represent westward (southward) GWMF, in (a) and (b), respectively.

propagation of the monsoon generated GWs from the low-latitude tropics to the high-latitude summer mesosphere.

In Figure 5, we compare the location (latitude) of the maximum GWMF at each pressure altitude from both SABER (Figure 2a) and NOGAPS-ALPHA (Figure 3a), calculated using equation (3). The location of maximum GWMF from both data and high-resolution model is generally constant with altitude up to ~1 hPa (~50 km). Above this altitude both SABER and NOGAPS-ALPHA show the GWMF tilting poleward with increasing altitude. The maximum GWMF at 0.01 hPa (~80 km) is at ~50°N. Above 80 km the location of maximum momentum flux from data and model diverge, with the maximum SABER flux extending to 80°N at ~84 km and the maximum model flux extending to 60-70°N near the model top. As noted above, the model forecast results have some biases above 80 km which might contribute to the divergence between the two sets of points at these altitudes. Nevertheless, the GWMF from both the data and high-resolution model confirm that the upward and eastward/northward propagating monsoon GWs indeed reach the high-latitude mesosphere and could thus play a role in modulating the mesospheric environment. Note that the gap in maximum GWMF values between ~50°N and 70°N does not imply an absence of GWs, but shows that the slope of the 'tilt' is shallow from ~0.012 hPa to ~0.011 hPa.

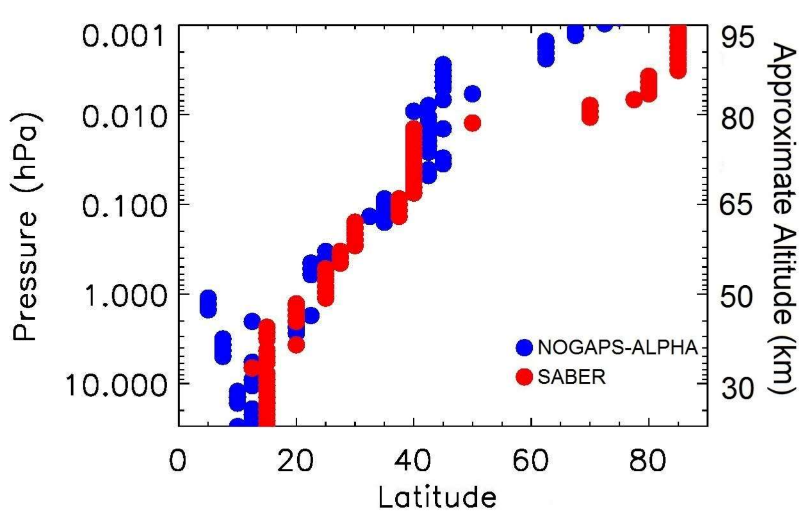

Figure 5. The location (latitude) of the maximum GWMF at each altitude from SABER and NOGAPS-ALPHA.

4. Role of Winds in the Oblique Propagation of GWs

As discussed in the introduction, gravity wave resolving models have shown that due to the latitudinal shear of the easterly winds, monsoon GWs can get refracted poleward and propagate obliquely from the tropical stratosphere to the high-latitude mesosphere. Since winds play an important role in this lateral propagation, here we analyze the influence of zonal winds on the filtering and propagation of monsoon GWs.

We show in Figure 6, the correlation coefficients between the time series of daily zonal mean GWMF at ~50 km, averaged over the NH tropics (15-30°N), and the global NOGAPS-ALPHA daily averaged absolute values of zonal winds (from the T79 analysis) at each altitude and latitude. The time series is restricted to the PMC season from late May to August (day of year (doy) 145 to 243 or 25 May to 31 August 2007) as this time period also coincides with the enhancement of the tropical stratospheric GW activity (not shown). *Wright and Gille* [2011] showed a clear relationship between the tropical stratospheric GW momentum flux using the High Resolution Dynamics Limb Sounder (HRDLS) data and monsoon activity (using rainfall data and outgoing longwave radiation as proxies), verifying that the monsoon region is the major

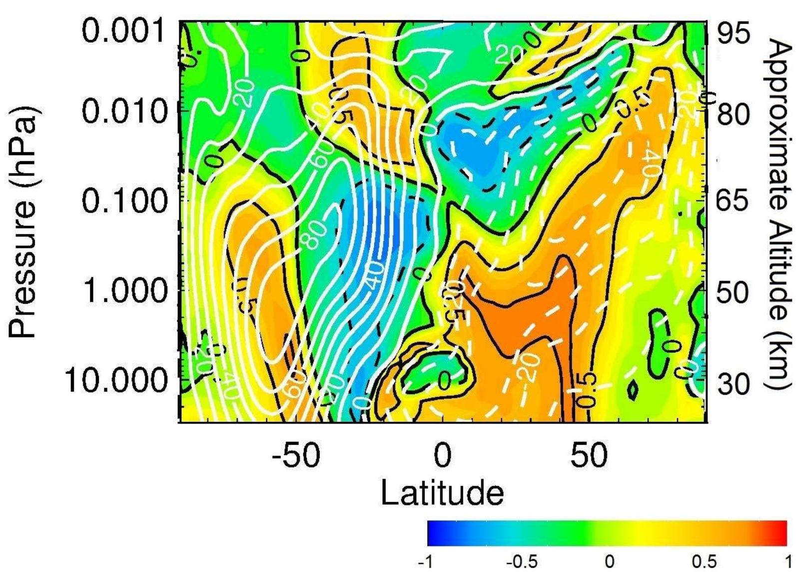

Figure 6. Latitude-altitude plot of correlation coefficients between time series of daily zonal mean 50 km monsoon GWMF and global NOGAPS-ALPHA zonal winds (see text for details). White contours indicate the easterly (dashed line) and westerly (solid line) zonal winds.

source of tropical stratospheric GW activity in summer. Note that although the official start date of the monsoon season over the Indian subcontinent is doy 148 or 28 May 2007 [*Wang* et al., 2009], in general, the onset of the Asian summer monsoon occurs over the Bay of Bengal in early May, advances northward, and covers the entire south east Asia by the end of May and India by mid-June [*Zhang* et al., 2004]. The African and the North American monsoon seasons usually starts in mid- to late- June. The NH monsoon season typically ends in late September to mid-October. However, since the NH stratospheric easterly winds reverse in late August, the westerly winds will filter the upward propagating easterly monsoon GWs thus shortening the stratospheric 'monsoon GW activity' to a time period similar to the PMC activity.

From Figure 6, in the SH, the westerly winds will prevent the eastward propagating monsoon GWs from propagating upward and therefore the correlations here are by chance and not relevant to this discussion. In the NH, above ~50 km, the high (>0.5) positive correlation coefficient (95% significant) extends from the tropics to the high latitude mesosphere, up to PMC altitudes (~84 km) between ~70-80°N. The slanted structure of this positive correlation follows the poleward tilt of the easterly winds. As examples, we show in Figure 7 the scatter between the GWMF at 50 km, 15-30°N and winds at three different altitudes and latitudes, (a) 50 km, 15-30°N (b) 65 km, 45-55°N, and (c) 80 km, 70-80°N, along the slanted structure. The correlation coefficient at all three locations is ~0.7. The slanted structure of the positive correlation coefficient along with the slanted GWMF structure in Figure 2 provides evidence of the oblique propagation of monsoon GWs and is consistent with the theory of wave focusing into

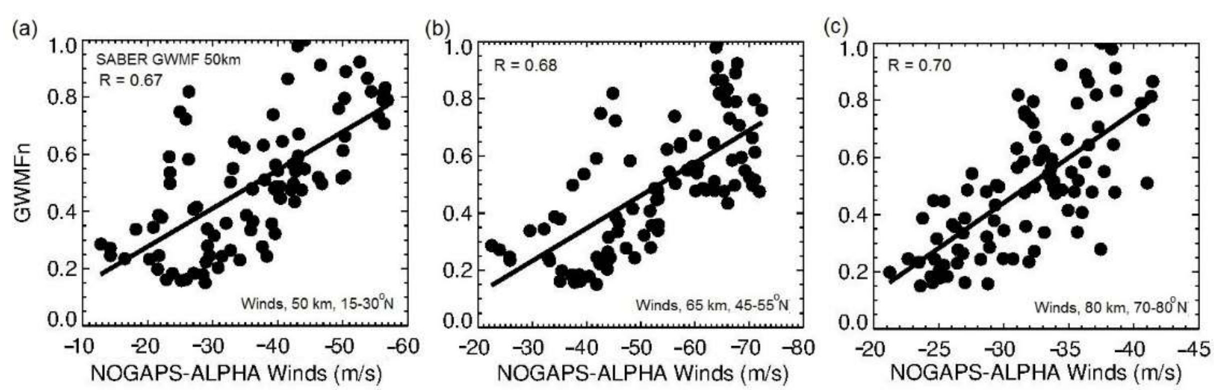

Figure 7. Scatter plot of normalized SABER GWMF at 50 km, 15-30°N and NOGAPS-ALPHA zonal winds at (a) 50 km, 15-30°N, (b) 65 km, 45-55°N, and (c) 80 km, 70-80°N.

the easterly jet. Those monsoon GWs that reach the high-latitude mesosphere will have some influence on the mesospheric environment. In Section 5, we use the PMC activity as an indicator of the variability of the summer mesospheric environment and further confirm the oblique propagation of GWs to the high-latitude mesosphere by analyzing the influence of the monsoon GWs on PMCs.

5. Effect of Monsoon GWs on PMCs

To determine the influence of monsoon GWs on the high-latitude mesosphere, we use PMC OF as an indicator of changes in the mesospheric environment. In Figure 8 we compare the zonal mean daily averaged time series of GWMFs at ~50 km, averaged over 15-30°N with the zonal mean daily averaged PMC OF time series at ~84 km, averaged over 65-85°N, over the NH 2007 PMC season. As mentioned earlier, CIPS observations indicate that the NH 2007 PMC season started on doy 145 [e.g. *Bailey et al*., 2009] and extended to doy 243 (25 May to 31 August 2007). The late season PMC activity during the NH 2007 PMC season has been attributed to the increase in quasi 5-day wave activity since doy 206 (25 July 2007) [*Nielsen et al*., 2010]. Nielsen et al. noted that although the zonal mean temperatures were above the frost point during the late NH 2007 PMC season, the 5-day wave activity peaked during this time, thus cooling the temperature and supporting the formation of bright PMCs in the troughs of the 5-day wave.

Figure 8 shows that, in general, the seasonal PMC variability, follows the 50 km monsoon GW activity during the same time period, with higher wave activity corresponding to increased cloud occurrence. As noted in Section 3, the 'start' of the 50 km monsoon GW activity is attributed to the start of the monsoon convective activity and the 'end' to the reversal of the easterly winds and filtering of the upward propagating GWs. The PMC OF and GWMF time series over the PMC season (doy 145-243) are significantly correlated with a correlation coefficient of 0.84. In Figure 8, some of the peaks and valleys in the GW time series, in the first half of the PMC season match those features in the PMC time series. The difference between PMC OF and GWMF from doy 206 to doy 243 is attributed to the influence of the quasi 5-day wave dominating over the influence of monsoon GWs. Accordingly, the correlation coefficient between PMC OF and GWMF from doy 143-205 is 0.97 and from doy 206-243 is 0.76.

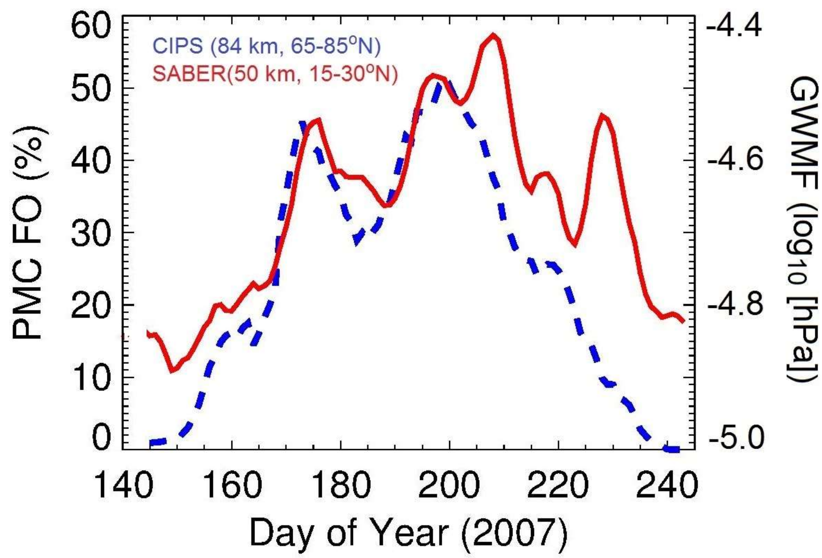

Figure 8. Time series of daily CIPS PMC occurrence frequency (blue dashed line) at 84 km, 65-85°N and SABER GWMF (red solid line) at 50 km, 15-30°N.

To support the fact that the correlation between monsoon GWs and PMCs is real and not a coincidence, we show in Figure 9 a contour plot of the correlation coefficients between the PMC time series shown in Figure 8 and the zonal mean daily averaged global GWMF time series at each altitude and latitude, for the same time period. We only consider the GW activity in the latitude range -50°S to 50°N to get a continuous data series during the time period of interest (SABER high-latitude data is interrupted by the satellite yaw cycle). The correlation coefficients are generally positive, with most of the negative values (not significant) in the SH mesosphere. The correlation coefficients with values greater than 0.7 are concentrated between ~50-65 km and 20-35°N, but correlation coefficients greater than 0.5 are also seen in the SH stratosphere and the NH mesosphere.

6. Discussion

There are two aspects of the correlation coefficients shown in Figure 9 that are interesting and which may motivate future work. First, the positive correlation between the monsoon GWs and PMCs means that an increase in monsoon GWs correlates with an increase in PMC

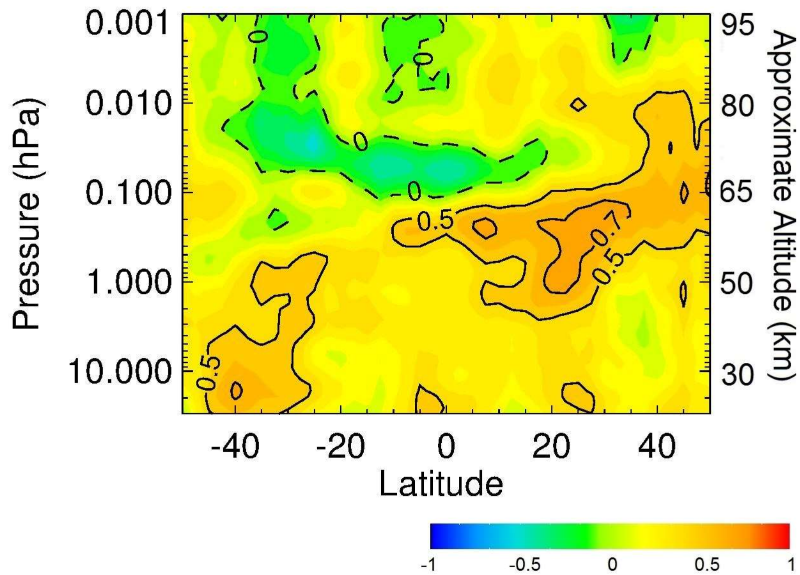

Figure 9. Latitude-altitude plot of correlation coefficients between daily averaged zonal mean time series of global GWMF and PMC OF.

occurrence frequency and vice versa. Therefore, these monsoon GWs may not necessarily be the same waves observed in the CIPS PMC images by, for e.g. *Chandran* et al. [2010], where the GW structures (or increased GW activity) are anti-correlated to the cloud occurrence frequency. The present study cannot answer the question as to the source of the GWs observed in the PMC data. They could be obliquely propagating monsoon generated GWs or vertically propagating waves from high latitude meteorological disturbances. For example, *Yue* et al [2014] argued that the source of the concentric wave structures seen in some CIPS images could be from thunderstorm activity in Siberia, although this was difficult to demonstrate with ray tracing.

A second interesting feature in Figure 9 is the presence of a significant correlation (> 0.5) in the winter hemisphere. It suggests a possible link between the winter time dynamics and the summer mesopause in the opposite hemisphere. This has been the subject of several studies that have the explored the link between planetary waves in the winter hemisphere and equatorial GWs and from there, the summer mesopause [*Karlsson* et al., 2007; *Karlsson* et al., 2009; *Kornich and Becker*, 2010]. This pattern of teleconnection from the southern winter to the northern summer of 2007 was observed by *Siskind* et al. [2011] and *Goldberg* et al. [2013]. More recently, a slightly different pathway of coupling from the winter hemisphere to the summer mesopause was identified by *Karlsson and Becker* [2016]. They showed how GWs in the winter hemisphere can impact the global mean meridional circulation and thus cool the summer mesopause. The question of whether the correlation in the SH seen in Figure 9 is due to winter planetary waves modulating the monsoonal GWs or, more directly, to vertically propagating winter GWs, (e.g. the mountain waves discussed by *Pautet* et al., [2016]), controlling the mean meridional circulation requires more detailed analysis and is beyond the scope of this study.

7. Summary and Conclusions

High-resolution gravity wave resolving models have revealed an oblique propagation of GWs in the summer hemisphere, from the stratosphere above the tropical monsoon convection source to the high-latitude mesosphere, indicating a new source of GWs in the summer polar mesosphere. Motivated by these modeling studies, here we presented a combination of satellite observation and modelling study of the oblique propagation of GWs during the NH 2007 summer. Global GW momentum flux and amplitude were derived from SABER temperature data. In July 2007, in the NH, the structure of the GWMF exhibits a poleward tilt, tilting from ~50 km, 15-30°N to ~84 km, 80°N. This tilted structure follows the slanted structure of the monsoon easterly jet in agreement with modeling studies. The GWMF calculated from the first 9-days of high-resolution (T479 forecast) NOGAPS-ALPHA temperatures also show the slanted structure. While this structure is more pronounced in the SABER momentum flux, the values of the momentum flux from both data and high-resolution model are in good agreement. Since GWMF derived from satellite temperature observations cannot provide the direction of wave propagation, we used the high-resolution (T479 forecast) NOGAPS-ALPHA model wind data to calculate the zonal and meridional components of the GWMF. The model results indicate that the GWs in the NH summer are eastward and northward propagating waves. These GW components also have the same tilted structure as seen in the absolute GWMF calculated from temperature.

The location (latitude) of the maximum GWMF in the NH from both SABER and NOGAPS-ALPHA high-resolution model agree up to ~80 km, 50°N. In the upper stratosphere (30-50 km) the location of this maximum is generally constant above the monsoon region. Above 50 km the maximum GWMF at each increasing altitude shifts poleward and exhibits a slanted structure. This structure extends to PMC altitudes (~84 km) and ~80°N in the SABER data, while it extends to >95 km, 80°N in the NOGAPS-ALPHA data. A significant positive correlation between daily averaged zonal mean time series of upper stratospheric, tropical GWs with the time series of global zonal winds (from the T79 NOGAPS-ALPHA analysis) show a slanted structure that coincides with the slanted easterly wind structure. Thus, despite the discrepancy between SABER data and the high-resolution NOGAPS-ALPHA forecast model, these results corroborate the modeling theory of refraction and poleward focusing of monsoon generated GWs into the easterly winds leading to the oblique propagation of these waves from the low-latitude stratosphere to the high-latitude mesosphere.

The monsoon GWs that reach the mesosphere will have some influence on the high-latitude summer mesosphere. Since PMCs are the most sensitive indicators of changes in the summer mesospheric environment, we analyzed the influence of monsoon generated GWs on the high-latitude mesosphere by correlating the daily averaged zonal mean time series of the 50 km SABER GWMF with the available PMC OF time series from the CIPS instrument, for the NH 2007 PMC season. The 50 km GWMF above the monsoon region is positively correlated with the PMC OF implying that the monsoon GWs do have some influence on the high-latitude summer mesosphere. The dissimilarity between the two time-series at the end of the PMC season is attributed to the influence of the quasi 5-day waves dominating over the influence of the monsoon GWs on PMCs. The significant positive correlation coefficients between the global GWMF and PMC OF extends from the SH stratosphere to the tropical upper stratosphere and the NH mesosphere. This suggests that the global circulation modulating the SH winter stratosphere could also be modulating the NH tropical stratosphere and high-latitude mesosphere in a similar fashion. More observational studies are needed to understand the relative roles of monsoon GWs, quasi 5-day planetary waves, and the coupling between hemispheres in influencing the summer polar mesosphere.

Acknowledgements

This work was supported by the NASA/AIM mission under contract NAS5-03132. AIM was developed as part of the NASA Small Explorer project. The authors acknowledge the SABER and CIPS science and data processing teams, the NOGAPS-ALPHA team and a grant of time from the DoD Supercomputing Resource Center. The SABER data are available online at

http://saber.gats-inc.com/index.php. The CIPS data are available online at http://lasp.colorado.edu/aim/index.html. The 6 hourly NOGAPS-ALPHA analysis is available via anonymous ftp at map.nrl.navy.mil in the aim9c subdirectory. The T479 NOGAPS-ALPHA forecast is available upon special request from the authors (DES).

References

Alexander, M. J. and T. J. Dunkerton, (1999), A spectral parameterization of mean-flow forcing due to breaking gravity waves, *J. Atmos. Sci*, 56, 4167-4182.

Alexander, M. J. et al. (2010), Recent developments in gravity-wave effects in climate models and the global distribution of gravity-wave momentum flux from observations and models. *Q. J. R. Meteorol. Soc.,* 136*,* 1103–1124. DOI:10.1002/qj.637

Alexander, M. J. (2015), Global and seasonal variations in three dimensional gravity wave momentum flux from satellite limb-sounding temperatures, *Geophys. Res. Lett.*, 42, 6860–6867, doi:10.1002/2015GL065234.

Andrews, D. G., J. R. Holton, and C. B. Leovy (1987), *Middle Atmosphere Dynamics*, 1st ed., Elsevier, New York.

Bailey, S.M., G. E. Thomas, D. W. Rusch, A. W. Merkel, C. Jeppesen, J. N. Carstens, C. E. Randall, W. E. McClintock, J. M. Russell III (2009), Phase functions of polar mesospheric cloud ice as observed by the CIPS instrument on the AIM satellite, *J. Atmos. Sol.-Terr. Phys* 71, 373–380, http://dx. doi.org/10.1016/j.jastp.2008.09.039.

Benze, S., et al., (2009), Comparison of polar mesospheric cloud measurements from the cloud imaging and particle size experiment and the solar backscatter ultraviolet instrument in 2007, *J. Atmos. Solar-Terr. Phys*. 71, 365–372, http://dx.doi.org/10.1016/j.jastp.2008.07.014.

Benze, S., et al., (2011), Evaluation of AIM CIPS measurements of polar mesospheric clouds by comparison with SBUV data, *J. Atmos. Solar-Terr. Phys*. 73 (14–15), 2065–2072, http://dx.doi.org/10.1016/j.jastp.2011.02.003.

Buhler, O., and M. E. McIntyre (2003), Remote recoil: A new wave-mean interaction effect, *J. Fluid Mech.*, 492, 207– 230.

Carstens, J. N., S. M. Bailey, J. D. Lumpe, J. D., C. E. Randall (2013), Understanding uncertainties in the retrieval of polar mesospheric clouds from the cloud imaging and particle size experiment in the presence of a bright Rayleigh background, *J. Atmos. Sol.-Terr. Phys*. 104, 197-212, doi:10.1016/j.jastp.2013.08.006

Chandran, A., et al. (2010), Polar mesospheric cloud structures observed from the cloud imaging and particle size experiment on the Aeronomy of Ice in the Mesosphere spacecraft: Atmospheric gravity waves as drivers for longitudinal variability in polar mesospheric cloud occurrence, *J. Geophys. Res.*, 115, D13102, doi:10.1029/2009JD013185.

Chu, X., C. Yamashita, P. J. Espy, G. J. Nott, E. J. Jensen, H.-L. Liu, W. Huang, and J. P. Thayer (2009), Responses of polar mesospheric cloud brightness to stratospheric gravity waves at the South Pole and Rothera, Antarctica, *J. Atmos. Sol.-Terr. Phys*., 71, 434–445, doi:10.1016/j. jastp.2008.10.002.

Dalin, P., S. Kirkwood, A. Moström, K. Stebel, P. Hoffmann, W. Singer, (2004), A case study of gravity waves in noctilucent clouds. *Ann. Geophys.,* 22, 1875–1884.

Eckermann, S. D., K. W. Hoppel, L. Coy, J. P. McCormack, D. E. Siskind, K. Nielsen, A. Kochenash, M. H. Stevens, and C. R. Englert (2009), High-altitude data assimilation system experiments for the Northern Hemisphere summer mesosphere season of 2007, *J. Atmos. Sol. Terr. Phys.*, *71*, 531–551.

Ern, M., P. Preusse, M. J. Alexander, and C. D. Warner (2004), Absolute values of gravity wave momentum flux derived from satellite data, *J. Geophys. Res*., 109, D20103, doi:10.1029/2004JD004752.

Ern, M., P. Preusse, J. C. Gille, C. L. Hepplewhite, M. G. Mlynczak, J. M. Russell, III, and M. Riese (2011), Implications for atmospheric dynamics derived from global observations of gravity wave momentum flux in stratosphere and mesosphere, *J. Geophys. Res*., 116, D19107, doi:10.1029/2011JD015821.

Forbes, J. M., et al. (1994), Semidiurnal tide in the 80–150 km region: An assimilative data analysis, *J. Atmos. Terr. Phys*., 56, 1237–1249.

Fritts, D. C., and M. J. Alexander (2003), Gravity wave dynamics and effects in the middle atmosphere, *Rev. Geophys*., 41(1), 1003, doi:10.1029/2001RG000106.

Garcia, R. R., and S. Solomon (1985), The effect of breaking gravity waves on the dynamics and chemical composition of the mesosphere and lower thermosphere, *J. Atmos. Sci.*, 90, 3850–3868.

Garcia, R. R., D. R. Marsh, D. E. Kinnison, B. A. Boville, and F. Sassi (2007), Simulation of secular trends in the middle atmosphere, 1950–2003, *J. Geophys. Res.*, 112, D09301, doi:10.1029/2006JD007485.

Garcıa-Comas, M., M. Lopez-Puertas, B.T. Marshall, P. P. Wintersteiner, B. Funke,1 D. Bermejo, Pantaleón, C. J. Mertens, E. E. Remsberg, L. L. Gordley, M.G. Mlynczak, and J.M. Russell III (2008), Errors in SABER kinetic temperature caused by non-LTE model parameters, *J. Geophys. Res*. 113, D24, doi: 10.1029/2008JD010105.

Gerrard, A. J., T. J. Kane, S. D. Eckermann, and J. P. Thayer (2004), Gravity waves and mesospheric clouds in the summer middle atmosphere: A comparison of lidar measurements and ray modeling of gravity waves over Sondrestrom, Greenland, *J. Geophys. Res*., 109, D10103, doi:10.1029/2002JD002783.

Goldberg, R. A., A. G. Feofilov, W. D. Pesnell, A. A. Kutepov (2013), Inter-hemispheric coupling during northern polar summer periods of 2002-2010 using TIMED/SABER measurements, *J. Atmos. Sol.-Terr. Phys*., 104, 277–284, doi:10.1016/j. jastp.2012.11.018.

Hasha, A., O. Buhler, and J. Scinocca (2008), Gravity wave refraction by three-dimensionally varying winds and the global transport of angular momentum, *J. Atmos. Sci.*, 65, 2892– 2906.

Hervig, M. E., U. Berger, D. E. Siskind (2016), Decadal variability in PMCs and implications for changing temperature and water vapor in the upper mesosphere, *J. Geophys. Res.*, 121, 2383-2392, doi:10.1002/2015JD024439

Holton, J. R., and M. J. Alexander (2000), The role of waves in the transport circulation of the middle atmosphere, in *Atmospheric Science Across the Stratopause, Geophys. Monogr. Ser.,* vol. 123, edited by D. E. Siskind, S. D. Eckermann, and M. E. Summers, pp. 21–35, AGU, Washington, D. C.

Holton, J. R., M. J. Alexander, and M. T. Boehm (2001), Evidence for short vertical wavelength Kelvin waves in the Department of Energy-Atmospheric Radiation Measurement Nauru99 radiosonde data, *J. Geophys. Res*., 106(D17), 20,125–20,129, doi:10.1029/2001JD900108.

Hoppel, K. W., N. L. Baker, L. Coy, S. D. Eckermann, J. P. McCormack, G. E. Nedoluha, and E. Siskind (2008), Assimilation of stratospheric and mesospheric temperatures from MLS and SABER in a global NWP model, *Atmos. Chem. Phys.*, 8, 6103–6116.

Huang, Y. Y., S. D. Zhang, F. Yi, C. M. Huang, K. M. Huang, Q. Gan, and Y. Gong (2013), Global climatological variability of quasi-two-day waves revealed by TIMED/SABER observations, *Ann. Geophys.*, 31, 1061–1075, doi:10.5194/angeo-31-1061-2013.

Innis, J., A. R. Klekociuk, R. J. Morris, A. Cunningham, A. Graham, D. J. Murphy, (2008), A Study of the Relationship between Stratospheric Gravity Waves and Polar Mesospheric Clouds at Davis, Antarctica, *J. Geophys. Res.*, 113, D14102, doi:10.1029/2007JD009031.

Jensen, E. J., and G. E. Thomas (1994), Numerical simulations of the effects of gravity waves on noctilucent clouds, *J. Geophys. Res.*, 99(D2), 3421–3430.

Jiang, J., B. Wang, K. Goya, K. Hocke, S. Eckermann, J. Ma, D. Wu, and W. Read (2004), Geographical distribution and interseasonal variability of tropical deep convection: UARS MLS observations and analyses, *J. Geophys. Res.*, 109, D03111, doi:10.1029/2003JD003756.

Kalisch, S., P. Preusse, M. Ern, S. D. Eckermann, and M. Riese (2014), Differences in gravity wave drag between realistic oblique and assumed vertical propagation, *J. Geophys. Res. Atmos.*, 119, 10,081–10,099, doi:10.1002/2014JD021779.

Karlsson, B., and E. Becker (2016), How does interhemispheric coupling contribute to cool down the summer polar mesosphere, *J. Clim*., 29, doi: http://dx.doi.org/10.1175/JCLI-D-16-0231.1

Karlsson, B., H. Körnich, H., and J. Gumbel (2007), Evidence for interhemispheric stratosphere-mesosphere coupling derived from noctilucent cloud properties, *Geophys. Res. Lett*., 34, L16806, doi:10.1029/2007GL030282.

Karlsson, B., C. McLandress, and T. G. Shepherd (2009), Inter-hemispheric mesospheric coupling in a comprehensive middle atmosphere model, *J. Atmos. Sol. Terr. Phys.*, 71(3–4), 518–530, doi:10.1016/j.jastp.2008.08.006.

Kim, Y.-J., S. Eckermann, and H.-Y. Chun (2003), An overview of the past, present and future of gravity-wave drag parametrization for numerical climate and weather prediction models, *Atmos. Ocean*, 41, 65–98.

Körnich, H. and R. Becker (2010), A simple model for the interhemispheric coupling of the middle atmosphere circulation, *Adv. Space Res*., 45, 661–668.

Li, J., and Q. Zeng (2002), A unified monsoon index, *Geophys. Res. Lett*., 29(8), 1274, doi:10.1029/2001GL013874.

Lindzen, R. (1981), Turbulence and Stress Owing to Gravity Wave and Tidal Breakdown, *J.*

Geophys. Res., 86 (C10), 9707–9714, doi:10.1029/JC086iC10p09707.

Liu, H.-L., J. M. McInerney, S. Santos, P. H. Lauritzen, M. A. Taylor, and N. M. Pedatella, (2014) Gravity waves simulated by high-resolution Whole Atmosphere Community Climate Model, *Geophys. Res. Lett.*, 41, 9106-9112, doi:1002/2014GL062468.

Lumpe, J. D., et al. (2013), Retrieval of polar mesospheric cloud properties from CIPS: Algorithm description, error analysis and cloud detection sensitivity, *J. Atmos. Sol.-Terr. Phys*. 104, 167-196, doi:10.1016/j.jastp.2013.06.007

McClintock, W., et al., (2009), The cloud imaging and particle size experiment on the aeronomy of ice in the mesosphere mission: Instrument concept, design, calibration, and on-orbit performance, *J. Atmos. Sol. Terr. Phys*., 71, http://dx.doi.org/10.1016/j.jastp.2008.10.011

Nielsen, K., D.E. Siskind, S.D. Eckermann, K.W. Hoppel, L. Coy, J.P. McCormack, S. Benze, C.E. Randall, and M.E. Hervig (2010), Seasonal variation of the quasi 5-day planetary wave: Causes and consequences for polar mesospheric cloud variability in 2007, *J. Geophys. Res*. 115, D18111, doi:10.1029/2009JD012676.

Pautet, P.-D., M. J. Taylor, D. C. Fritts, K. Bossert, B. P. Williams, D. Broutman, J. Ma, S. D. Eckermann, J. D. Doyle (2016), Large-amplitude mesospheric response to an orographic wave generated over the Southern Ocean Auckland Islands (50.7°S) during the DEEPWAVE project, *J. Geophys. Res. Atmos*., 121, 1431–1441, doi:10.1002/2015JD024336.

Preusse, P., A. Dörnbrack, S. D. Eckermann, M. Riese, B. Schaeler, J. T. Bacmeister, D. Broutman, and K. U. Grossmann (2002), Space-based measurements of stratospheric mountain waves by CRISTA: 1. Sensitivity, analysis method, and a case study, *J. Geophys. Res*., 107(D23), 8178, doi:10.1029/2001JD000699.

Preusse, P., et al. (2006), Tropopause to mesopause gravity waves in August: Measurement and modeling, *J. Atmos. Sol. Terr. Phys*., 68, 1730–1751, doi:10.1016/j.jastp.2005.10.019.

Preusse, P., S. D. Eckermann, M. Ern, J. Oberheide, R. H. Picard, R. G. Roble, M. Riese, J. M. Russell III, and M. G. Mlynczak (2009), Global ray tracing simulations of the SABER gravity wave climatology, *J. Geophys. Res*., 114, D08126, doi:10.1029/2008JD011214.

Rapp, M., F.-J. Lübken, A. Müllemann, G. E. Thomas, and E. J. Jensen (2002), Small-scale temperature variations in the vicinity of NLC: Experimental and model results, *J. Geophys. Res*., 107(D19), 4392, doi:10.1029/2001JD001241.

Remsberg, E. E., et al. (2008), Assessment of the quality of the Version 1.07 temperature versus-pressure profiles of the middle atmosphere from TIMED/SABER, *J. Geophys. Res*. 113, D17101, doi:10.1029/2008JD010013.

Richter, J. H., F. Sassi, and R. R. Garcia (2010), Towards a physically based gravity wave source parameterization in a general circulation model, *J. Atmos. Sci.*, 67, 136–156.

Rusch, D.W., et al., (2009), The cloud imaging and particle size experiment on the aeronomy of ice in the mesosphere mission: Cloud morphology for the Northern 2007 season, *J. Atmos. Sol. Terr. Phys*., 71, 356–364, http://dx.doi.org/10.1016/j.jastp.2008.11.005.

Russell, J. M., III, M. G. Mlynczak, L. L. Gordley, J. Tansock, and R. Esplin (1999), An overview of the SABER experiment and preliminary calibration results, in *Proceedings of the SPIE*, 44th Annual Meeting, 3756, 277–288, Denver, Colo., 18–23 July.

Sato, K., M. Yamamori, S.-Y. Ogino, N. Takahashi, Y. Tomikawa, and T. Yamanouchi (2003), A meridional scan of the stratospheric gravity wave field over the ocean in 2001 (MeSSO2001), *J. Geophys. Res*., 108(D16), 4491, doi:10.1029/2002JD003219.

Sato, K., S. Watanabe, Y. Kawatani, Y. Tomikawa, K. Miyazaki, and M. Takahashi (2009), On the origins of mesospheric gravity waves, *Geophys. Res. Lett*., 36, L19801, doi:10.1029/2009GL039908.

Salby, M. L. (1981), The 2-day wave in the middle atmosphere: Observations and theory, *J. Geophys. Res*., 86(C10), 9654–9660, doi:10.1029/JC086iC10p09654.

Siskind, D. E., S. D. Eckermann, J. P. McCormack, M. J. Alexander and J. T. Bacmeister, (2003), Hemispheric differences in the temperature of the summertime stratosphere and mesosphere, *J. Geophys. Res*., 108, D2, 4051, doi:10.1029/2002JD002095.

Siskind, D. E., M. H. Stevens, M. Hervig, F. Sassi, K. Hoppel, C. R. Englert, A. J. Kochenash (2011), Consequences of recent Southern Hemisphere winter variability on polar mesospheric clouds, *J. Atmos. Sol.-Terr. Phys*, 73,2013 – 2021.

Siskind, D. E. (2014), Simulations of the winter stratopause and summer mesopause at varying spatial resolutions, *J. Geophys. Res. Atmos*., 119, doi:10.1002/2013JD020985.

Thomas, G.E., J. J. Olivero, E. J. Jensen, W. Schröder, O. B. Toon (1989), Relation between increasing methane and the presence of ice at the mesopause, *Nature,* 338, 490–492.

Thomas, G.E., J. J. Olivero, M. DeLand, E. P. Shettle, (2003), Comment on are noctilucent clouds truly a ‘miner’s canary’ for global change?, *EOS Transactions*, American Geophysical Union, 84, 352–353.

Thurairajah, B., S. M. Bailey, K. Nielsen, C. E. Randall, J. Lumpe, M. J. Taylor, J. M. Russell III (2013), Morphology of polar mesospheric clouds as seen from space, *J. Atmos. Sol.-Terr. Phys*., 104, pp 234-243, doi:10.1016/j.jastp.2012.09.009.

Thurairajah, B., S. M. Bailey, C. Y. Cullens, M. E. Hervig, J. M. Russell III (2014), Gravity wave activity during recent stratospheric warming events from SOFIE temperature measurements, *J. Geophys. Res. Atmos,* 119, doi:10.1002/2014JD021763.

von Zahn, U. (2003), Are noctilucent clouds truly a ‘‘miner’s canary’’ of global change?, *EOS Transactions*, American Geophysical Union, 84 (28), pp. 261-264

Wang, B., Q. Ding, and P. V. Joseph (2009), Objective definition of the Indian summer monsoon onset, *J. Clim*., 22, 3303-3316, doi:10.1175/2008JCLI2675.1

Watanabe, S., Y. K awatani, Y. Tomikawa, K. Miyazaki, M. Takahashi, and K. Sato, (2008), General aspects of a T213L256 middle atmosphere general circulation model, *J. Geophys. Res*., 113, D12110, doi:10.1029/2008JD010026.

Wright, C. J., and J. C. Gille (2011), HIRDLS observations of gravity wave momentum fluxes over the monsoon regions, *J. Geophys. Res*., 116, D12103, doi:10.1029/2011JD015725.

Wu, D. L., P. B. Hays, W. R. Skinner, A. R. Marshall, M. D. Burrage, R. S. Lieberman, and D. A. Ortland (1993), Observations of the quasi 2-day wave from the high resolution Doppler imager on UARS, *Geophys. Res. Lett.*, 20(24), 2853–2856, doi:10.1029/93GL03008.

Wu, D. L., P. Preusse, S. D. Eckermann, J. H. Jiang, M. de la Torre Juarez, L. Coy, and D. Y. Wang (2006), Remote sensing of atmospheric gravity waves with satellite limb and nadir techniques, *Adv. Space Res*., 37, 2269–2277, doi:10.1016/j.asr.2005.07.0312.

Yamashita, C., S. L. England, T. J. Immel, and L. C. Chang (2013), Gravity wave variations during elevated stratopause events using SABER observations, *J. Geophys. Res. Atmos*., 118, 5297–5306, doi:10.1002/jgrd.50474

Yasui, R., K. Sato, and M. Tsutsumi (2016), Seasonal and Interannual Variation of Mesospheric Gravity Waves Based on MF Radar Observations over 15 Years at Syowa Station in the Antarctic, *SOLA*, vol. 12, 46-50, http://doi.org/10.2151/sola.2016-010.

Yue, J., B. Thurairajah, L. Hoffmann, J. Alexander, A. Chandran, M. J. Taylor, J. M. Russell III, C. E. Randall, and S.M. Bailey (2014), Concentric gravity waves in polar mesospheric clouds from the Cloud Imaging and Particle Size experiment, *J. Geophys. Res. Atmos*., 119, 5115–5127, doi:10.1002/2013JD021385.

Zhang, Z., J. C. L. Chan, and Y. Ding (2004), Characteristics, evolution and mechanisms of the summer monsoon onset over southeast Asia, *Int. J. Climatol*., 24, 1461-1482, doi: 10.1002/joc.1082.